Biochemical Pharmacology, Vol. 40, No. 1, pp. 7–13, 1990.
Printed in Great Britain.

0006-2952/90 $3.00 + 0.00

MOTIONAL EFFECTS ON NMR STRUCTURAL DATA

COMPARISON OF SPINACH AND *ESCHERICHIA COLI* ACYL CARRIER PROTEINS

YANGMEE KIM,* JOHN B. OHLROGGE† and JAMES H. PRESTEGARD‡

*Chemistry Department, Yale University, New Haven, CT 06511; and †Department of Botany and Plant Pathology, Michigan State University, East Lansing, MI 48824, U.S.A.

Abstract—Proteins in solution need not exist in a single rigid structure but can exist in a dynamic equilibrium among structural forms. The problems that this poses for structure determination using nuclear Overhauser effect data from two-dimensional NMR experiments are discussed and illustrated with data on functionally equivalent proteins from two different species. One of these proteins, acyl carrier protein from *Escherichia coli*, shows a single set of resonances, easily interpreted on the basis of a single rigid structure. However, the related protein, acyl carrier protein from spinach, shows two sets of resonances, suggesting that two conformers in dynamic equilibrium would be a better structural model.

Determination of protein structures on the basis of NMR-derived interproton distance constraints is now a well established science [1–6]. The structures derived to date, which are confined to relatively small proteins, show moderately high resolution and, in most cases, good agreement with X-ray structures [3, 5, 7, 8]. Yet, there are cases of discrepancies which cannot be dismissed easily, and there are cases where NMR structures, or parts of NMR structures, remain poorly defined despite the availability of high quality data [4]. In these cases we believe that it is important to consider the possibility that the assumption of a static structure, implicit in most structure determination protocols, is inappropriate. NMR is, after all, unique in providing structural data in solution where motional variations are less restricted than in crystals. The nuclear Overhauser effects (NOEs)§ used to evaluate interproton distance constraints are also susceptible to large variations because of the unusual way that motional averaging can affect the measured parameters.

In this paper, we illustrate the range of effects that motion can have on NMR data and NMR-derived structures by comparing results on a protein isolated from two different species. This protein is acyl carrier protein (ACP), an essential component of the fatty acid synthetase system in most organisms [9–12]. Where it is a soluble component of the system, it is a highly acidic molecule of approximately 80 amino acids. In all cases the sequences show structural homologies which favor extensive regions of α-helix, and in all cases a prosthetic group, which serves as the covalent link to a growing fatty acid chain, is attached to a serine near the mid-point of the sequence.

The proteins to be examined here are from *Escherichia coli* and from spinach.‖ The structure of the *E. coli* protein has been determined by NMR methods but shows regions with inconsistencies in constraint data, suggesting a possible motional anomaly [13]. The spinach protein has not as yet yielded to a complete structure determination, but it has been cloned and put into an expression vector capable of providing an adequate quantity of protein to pursue a structure [14]. Preliminary data on this protein will be presented here which suggest a strong structural homology with the *E. coli* protein but a shift to slower time scales of conversion between alternate conformers. This allows a direct comparison of effects on NMR data which exist for both fast and slowly exchanging systems.

THEORY

In comparison to techniques like X-ray diffraction, NMR has a very slow time scale of measurement. If conformers interconvert at a rate that is rapid compared to the frequency separation of resonances for a given proton in each conformer (typically tens to hundreds of Hz), a single, averaged resonance will be observed. Relaxation properties, measured as NOE transfers involving the proton, will also be averaged between the two states. The single resonance and averaged relaxation properties make it difficult to detect the presence of conformational equilibria. Stability limits for many proteins also prevent use of temperature to slow motions to ranges where discrete resonances (or broadening of a single resonance) occur.

Within the range where a single resonance for each proton is observed, a number of effects on relaxation properties can occur. In the limit of a rigid molecule, one assumes that there is only one motion modulating interproton interaction, namely Brownian diffusion of an approximately spherical object. The

‡ Corresponding author.

§ Abbreviations: NOE, nuclear Overhauser effect; ACP, acyl carrier protein; SDS–PAGE, sodium dodecyl sulfate–polyacrylamide gel electrophoresis; NOESY, nuclear Overhauser effect spectroscopy; and ROESY, rotating frame Overhauser spectroscopy.

‖ There are two distinct forms of ACP in spinach which have different amino acid sequences and different properties. Here we refer to spinach ACP-I which is the main protein in spinach.

cross-relaxation rate (σ_{ij}) dominating the early portions of transfer between a pair of protons, after perturbing one proton, displays an inverse sixth power dependence on the interproton distance (r_{ij}). This sixth power dependence arises because relaxation rates are proportional to the square of the interaction leading to relaxation, and in the case of the dipole–dipole interaction applicable to protons, the interaction depends on the inverse cube of the distance. The proportionality constant relating relaxation rates to $(1/r)^6$ is identical for each pair in the rigid model, allowing use of a known calibration distance to eliminate the constant. Unknown distances, therefore, can be calculated from observed cross-relaxation effects as follows:

$$\frac{\sigma_{ij}}{\sigma_{\text{ref}}} = \left(\frac{r_{\text{ref}}}{r_{ij}}\right)^6 \tag{1}$$

As a contrast to this rigid model, let us consider effects that occur with very rapid internal motion, namely motion that is rapid compared to the isotropic tumbling time of the whole molecule. The dipole–dipole interaction dependent on r^{-3} is, in this case, averaged before it is modulated by isotropic tumbling. One might anticipate a distance dependence of cross-relaxation rate, in which short distances of approach between two protons would be weighted heavily, $\langle r^{-3}\rangle^2$ and cross-relaxation rates would be enhanced. An angular part of the dipole–dipole interaction, however, is also averaged, and enhancement due to the $\langle r^{-3}\rangle^2$ part is nearly cancelled [15]. Therefore, except in cases of highly correlated motions, we can use a simple r^{-6} dependence of cross-relaxation and an isotropically tumbling rigid model to deduce reasonable structures for systems with only rapid internal motions.

Let us next consider a type of departure from a rigid model which involves motions that are slow compared to those which are effective in modulating relaxation interactions ($\tau_c > 10^{-8}$ sec) and yet fast compared to times which lead to resonance position averaging ($\tau_c < 10^{-3}$ sec). Here relaxation effects in each state are averaged as follows:

$$\sigma_{\text{eff}} = \sum_i p_i \sigma_i \tag{2}$$

where p_i is the probability of finding each state and σ_i is the cross-relaxation rate in each state. This type of averaging has a tendency to weight short distances of approach very severely, since the distance dependence is $\langle 1/r^6\rangle$ and not $\langle 1/r^3\rangle^2$. Also, there is no compensation by angular factors since the angular modulations from the slow motions are insignificant compared to the angular modulation from the faster isotropic tumbling.

Effects of interpreting data on the basis of a rigid model are more severe in this intermediate motion case. Consider the structural implication of interpreting a measured, average cross-relaxation rate, in terms of a single rigid model for the three nuclei labeled A, B, and C in Fig. 1. Let B spend one-half its time 3 Å from A and one-half its time 3 Å from C. If A and C are constrained by other factors to be 9 Å apart, the NOEs between A and B, as well as B and C, would be

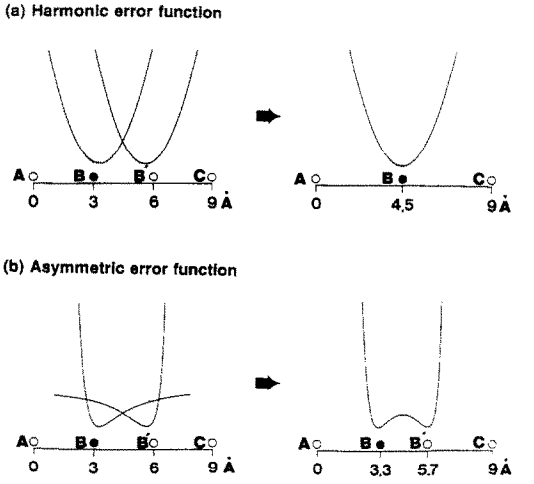

Fig. 1. Comparison of a harmonic error function and an asymmetric error function in the presence of averaging. Each circle shows the position of the nuclei.

$$\tfrac{1}{2}\,\text{Const}\,(\tfrac{1}{3})^6 + \tfrac{1}{2}\,\text{Const}\,(\tfrac{1}{6})^6 = \sigma_{\text{eff AB}}\sigma_{\text{eff BC}} \tag{3}$$

Interpreting this as a distance in a single conformer, we would find 3.3 Å, a value indicating B is very close to both A and C. This is clearly incompatible with the long AC distance constraint. This type of incompatibility can result in structures which appear to be poorly defined, or worse, which inaccurately represent the structure of the molecule.

Structure determination protocols frequently impose constraints using square well or harmonic error functions such as those depicted for the data in Fig. 1a [3, 16]. These error functions are summed over all constraints, and a structure is sought which minimizes the total function. It is clear from Fig. 1a that the protocol would find a compromise position 4.5 Å from A and C. While there would be a penalty assigned that should alert the investigator to the presence of a problem, the common practice of evaluating the quality of a structure based on convergence to a single minimum would not necessarily indicate a problem.

An alternative protocol uses an error function which more accurately represents NOE errors [17].

$$E_{\text{pseudo}} = W\left[\frac{1}{r_{ij}^3} - \frac{1}{r_{oij}^3}\right]^2 \tag{4}$$

Here W is a weighting factor (kcal/mol), r_{oij} is the distance in angstroms extracted from NOE data using a rigid model, and r_{ij} is the distance calculated from the coordinates of a trial structure. This asymmetric error function is soft on the long side as seen in Fig. 1b, and when two such error functions are superimposed they yield a double minimum as shown in Fig. 1b. When structures are sought starting at different points, the solutions tend to fall into two classes: those with B at 3.3 Å from A and those with B at 5.7 Å from A. The divergence in structures is easily seen in regions of molecules undergoing averaging. The individual families also serve as good starting points for structure determination protocols which explicitly recognize multiple conformers [13].

MATERIALS AND METHODS

Purification of spinach ACP

Spinach ACP-I was purified from *E. coli* strain E103S as previously described [14]. The preparation was judged homogeneous by electrophoresis on both native and SDS–PAGE.

Preparation of spinach palmitoyl-ACP

Spinach palmitoyl-ACP-I was prepared by acylation of 2 mg of spinach ACP-I using *E. coli* acyl-ACP synthetase [18]. The palmitoyl-ACP-I was isolated from the reaction mixture by chromatography on DEAE cellulose and from untreated ACP-SH by gel filtration on a Superose 12 FPLC column (Pharmacia) at pH 9.5.

NMR sample preparation

For non-acylated samples spinach ACP was reduced with dithiothreitol (DTT) to the free sulfhydryl form by adding 1.0 mg DTT to a 0.4-mL sample of 7 mM ACP-I at each pH and allowing it to react overnight. To change the pH of the sample, spinach ACP was passed through a Sephadex G-25 column with 1.2 mM phosphate buffer at the appropriate pH. Approximately 18 mL of eluent was collected, and this volume was reduced to 0.4 mL to give a final pH which is 0.5 lower than the original pH and a final buffer concentration of 50–55 mM. Palmitoyl-ACP samples were prepared in a similar manner except that DTT was omitted. Two equivalents of $MgCl_2$ were added to some samples to determine the effect of divalent ion content. Because of solubility problems in the presence of Mg^{2+}, 35 mM phosphate buffer was used instead of 50 mM in the presence of Mg^{2+}.

Samples for NMR measurement were lyophilized and dissolved in D_2O or 90% H_2O/10% D_2O, 50 mM phosphate buffers at the appropriate pH. Concentrations of protein were approximately 7 mM, for 2D experiments and 1 mM for 1D experiments. Sample volumes were approximately 0.4 mL.

NMR spectroscopy

NMR spectra were recorded on a Bruker AM 500 spectrometer or a 490 MHz home-built spectrometer. NOESY spectra [19] in water were recorded in the phase-sensitive mode using the method of States *et al.* [20], and NOESY spectra in D_2O were recorded in the pure-phase absorption mode using the time proportional phase incrementation method [21, 22]. In all cases a mixing time of 180 msec was used. Relay experiments were recorded as absolute magnitude spectra with mixing times of 18 msec [23]. All two-dimensional (2D) spectra were collected as 400–500 t_1 experiments, each with 2 K complex data points over a spectrum sweep width of 6024 Hz (sample in water) or 5000 Hz (sample in D_2O). Data were processed in a Vax 3200 computer with the FTNMR software program.* Data sets were multiplied in both dimensions by sine-bell functions or shifted sine-bell functions.

* FTNMR is a program licensed from Hare Research Inc., Woodinville, WA.

CD spectroscopy

A sample of spinach ACP was prepared for CD spectra at a concentration of 135 μM. Spectra were acquired with an AVIV model 60DS spectropolarimeter using a 1 mm cell. The base line was corrected with the same concentrations of phosphate buffer and DTT as in the spinach ACP solution. Spectra in the UV wavelength range from 200 to 260 nm showed molar elipticities -1.23×10^6 deg M^{-1} cm^{-1} at 220 nm. These were analyzed using the program PROSEC (protein secondary structure estimator) tailored to work directly with data recorded by the AVIV 60DS CD spectrometer [24] to yield 43% of α-helix.

RESULTS AND DISCUSSION

E. coli *ACP*

The structure of *E. coli* ACP has been determined using a molecular mechanisms pseudoenergy approach that employs asymmetric NMR potentials [4] and using a simulated annealing approach that employs harmonic potentials [25, 26]. Those structures were calculated on the basis of a single rigid model. The results, particularly using the asymmetric potential, show a large divergence among structures [4]. For example, Phe 50 is observed to have strong NOEs involving Ile 3, Leu 46 and Ile 72. All structures violate one or more of these NOEs by having an interproton distance which is too long to give rise to the observed NOE. Observation of effective cross-relaxation among protons at distant sites is precisely the type of artifact expected from averaging of NOEs over two or more discrete structures. Use of a two-state averaging model results in a dramatic improvement in fit to cross-relaxation-derived distance constraints and a substantial lowering of molecular mechanics energies for individual conformers of *E. coli* ACP [13].

Despite the improvement with a two-state model interpretation, evidence for conformational averaging is open to argument, because it is difficult to separate errors that result from mistakes in assignment, and the presence of other relaxation contributions, from errors that are associated with using the wrong motional model. It would be very desirable to have independent verification of the existence of multiple conformational states.

Spinach ACP

Structural variation among functionally identical proteins, isolated from different species, certainly occurs. But if one considers that a 1.4 kcal variation in residue–residue interaction frequently results in indiscernible movements of protein segments (<0.1 Å), but a 1.4 kcal variation in an activation barrier will result in an order of magnitude variation in rate, it is far more likely that we will detect variations in motional processes than variations in structural details. We believe this to be the case in comparing spinach ACP to *E. coli* ACP.

Structurally these two proteins are expected to be quite similar [9, 27]. Of 77 residues that overlap between *E. coli* and spinach ACP-I, 30 match exactly. Allowing conservative substitutions such as

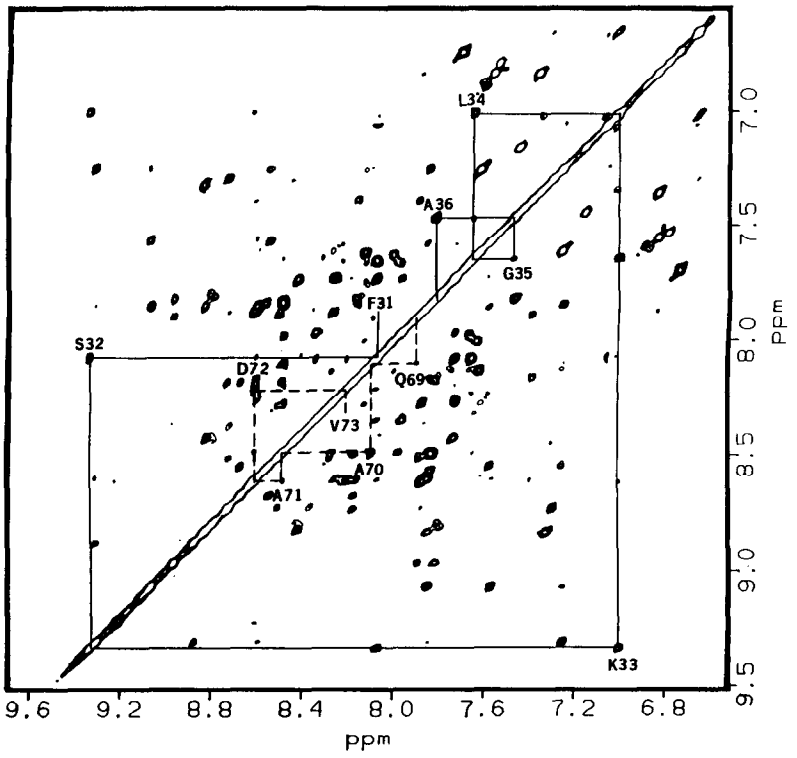

Fig. 2. Regions of a 490 MHz ^{1}H NOE spectrum of spinach ACP, pH 5.9 in water, containing amide–amide proton connectivities. This spectrum was acquired with a mixing time of 180 msec. The sequential assignments are shown with lines.

Glu/Asp, Ile/Val/Leu, and Thr/Ser gives an additional 10 matches or 51% homology. Allowing minor shifts in sequence such as required in correlating the highly conserved Phe residue at position 31 of spinach with the Phe residue at position 28 in *E. coli*, homology is improved further. Chou–Fasman predictions [28–30] of secondary structure are quite similar for the two proteins except at the C-terminus [31], and CD results show a similar level of α-helices. In spinach ACP there appears to be 43% of α-helical structure, while in *E. coli* ACP there appears to be 33–42% of α-helical structure [32, 33]. It has also been observed that *E. coli* ACP is an effective cofactor for the spinach fatty acid synthetase system [11], and antibodies raised against spinach ACP cross-react with *E. coli* ACP [27].

Structural homology is confirmed by NMR investigation. The amide–amide segments of a 2D NOESY spectrum is shown in Fig. 2. The off-diagonal connectivity peaks in this region are very characteristic of α-helices. The intensity of a crosspeak is directly related to σ for short mixing times and, therefore, the appearance reflects short amide–amide distances. In an α-helix, sequential amides are at 2.8 Å compared to ~3.5 Å in an extended sheet [34].

Complete sequential assignment now under way should localize helical regions within the sequence and further strengthen the structural homology model. However, even at the present level of assignment there are some anomalies. There are, for example, too many NOE connectivity peaks in some regions and some major peaks lack expected intensity. This is most easily seen in the aromatic spectral region of a sample in D_2O where only nonexchangeable protons remain. At the bottom of Fig. 3, there is a one-dimensional spectrum of spinach ACP at pH 6.0, 303°K. Spinach ACP has only resonances from two phenylalanines showing in the 6.6–7.6 ppm region. There should be 10 protons in this region. Peaks labeled C1, C2 and D clearly correspond to peaks expected for the A_2B_2X five spin system of one phenylalanine. But the integral of these peaks, if referenced to what must be the remaining 5 protons in peaks A and B, is low by more than 10%.

The assignments of the major peaks in Fig. 3 can be confirmed on the basis of a RELAY experiment shown in Fig. 4. The connectivities shown in solid lines are based solely on through bond couplings. Peaks C1, C2 and D must belong to ortho, meta and para protons on one phenylalanine. Based on NOE connectivities to other amino acids, this is Phe 31. Peaks A and B must, therefore, belong to ortho, and meta plus para protons on Phe 52. The peaks indicated with arrows are the crosspeaks from the amide peaks of side chains of glutamine and asparagine which were not exchanged in the H_2O sample used for this experiment.

Going back to Fig. 3, the NOE spectrum, we should expect connectivities between the spatially proximate ortho and meta protons, and para and

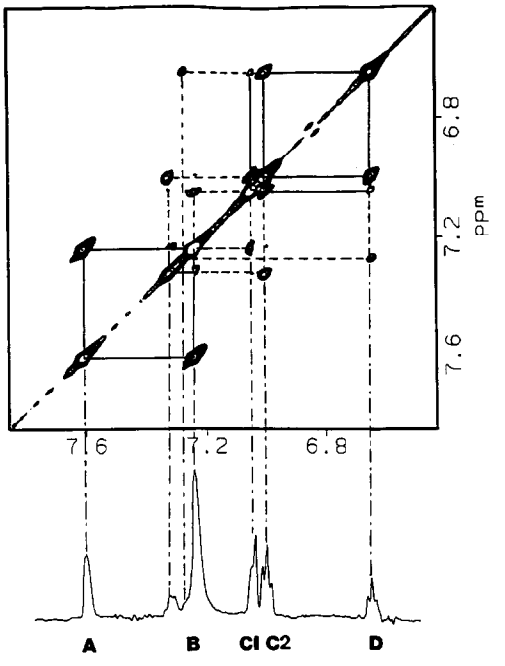

Fig. 3. The 500 MHz 2D NOESY spectrum and the 1D spectrum of the aromatic region of spinach ACP at pH 6.0 in D_2O. The solid lines show the expected intraresidue connectivities and dotted lines show extra connectivities. The solid–dotted lines correlate crosspeak positions with the positions of each peak in a 1D spectrum.

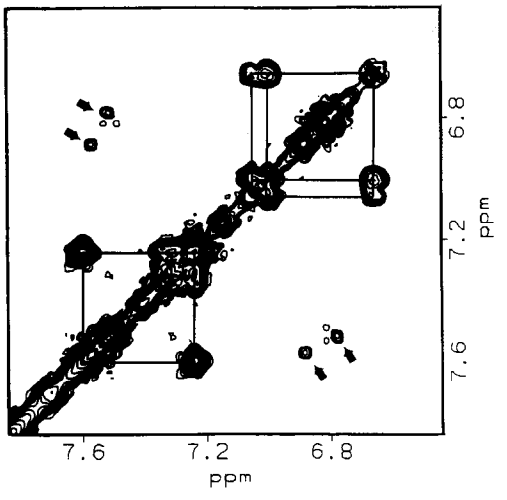

Fig. 4. RELAY spectrum of the aromatic region of spinach ACP at pH 6.3 in water. The solid lines show the through bond couplings of Phe 52 and Phe 31.

meta protons. Even some weak secondary transfers between para and ortho protons on the same ring are expected. Crosspeaks from expected transfers are shown with solid lines in the figure. Clearly there are additional crosspeaks. The dotted lines in Fig. 3 appear to show NOE connectivities from Phe 52 to Phe 31. While a remote interresidue connectivity is not impossible, it would require substantial distortion of the spinach structure from the *E. coli* ACP structure. Closer examination also shows that the positions of the extra crosspeaks do not correlate exactly with positions of major assigned resonances.

Changing environmental conditions can help resolve ambiguities in the observed connectivities by shifting and changing the intensity of peaks which may be present. For example, adding a palmitoyl chain to the prosthetic group serves to resolve the peak A, assigned to Phe 52, into two peaks, as shown in Fig. 5. This is also true for peak D, assigned to Phe 31. As a first explanation, it would be logical to assume that the extra peaks resulted from incomplete acylation, but HPLC shows >90% purity of the acyl form. Also in Fig. 5 we show the effects of varying pH, temperature and divalent ion content. Shifts in peak positions are not large in the range investigated, but peak areas do change. When the area of the upfield part of peak A increases, the downfield part decreases. Likewise, when the downfield part of peak D decreases, the upfield part increases. These changes are entirely reversible. This is characteristic of seeing discrete resonances for two conformers with the equilibrium population between them shifting back and forth with changes in environmental conditions, i.e. there are two conformers in slow exchange.

The extra peaks in the NOE spectra and the low intensity for Phe 31 in the 1D spectrum in Fig. 3 can now be explained. Although individual lines in the non-acylated species are not easily resolved, we suspect these are peaks from a minor second species underlying the primary resonances. NOE spectra measure transfer of magnetization from one resonance to another but do so independent of mechanism. Magnetization can show up as a crosspeak both when resonances physically exchange as in a conformational equilibrium, and when transfer is by dipolar relaxation mechanisms.

Consider the connectivities to the para proton of the Phe 31 peak D. Relaxation transfers intensity to a peak from the two meta protons, peak C2, and a small amount (probably secondary NOE) to a peak from the ortho proton, peak C1. But there is a strong transfer to a peak just downfield of peak B. This peak is not a part of either major spin system as established by scalar coupling and is certainly a second species connected to the main peaks by exchange. Similar extra peaks for the ortho and meta resonances of Phe 31 lie under peak B and show transfers to C1 and C2. There are experiments such as the ROESY experiment [35–37] that can separate exchange from true NOE transfers to confirm this explanation.

Figure 6 shows the effects of varying temperature and the addition of divalent ion on one-dimensional spectra of spinach-SH ACP. With the region just downfield of peak B assigned to resonances from a minor species, we can now clearly see resonance intensity shift from peaks C1, C2 and D to this region.

CONCLUSION

We believe we have presented adequate evidence to state that spinach ACP exists in at least two

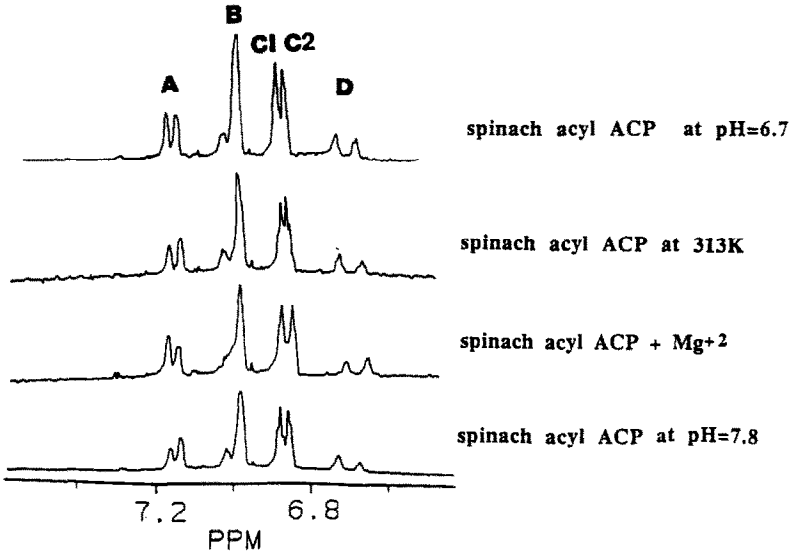

Fig. 5. Effects of varying pH, temperature and divalent ion content on palmitoyl-spinach ACP.

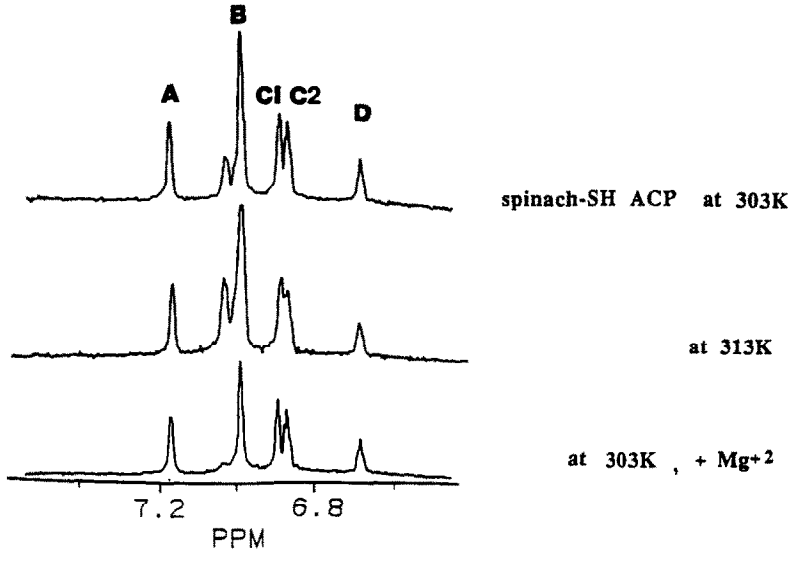

Fig. 6. Effects of varying temperature and divalent ion content on spinach-SH ACP.

conformationally discrete forms that exchange slowly enough to give discrete resonances, yet fast enough to transfer magnetization on the time scale of T_1 relaxation (1–2 sec). The observation of discrete conformational states in one species adds credence to the use of a conformational averaging model in the structure of *E. coli* ACP. The observations also caution against the indiscriminate use of a rigid model to analyze NMR data which gives a single resonance for each distinct proton site.

Acknowledgements—This work was supported by a research grant from the National Institutes of Health (GM 32243).

REFERENCES

1. Braun W, Wider G, Lee KH and Wüthrich K, Conformation of glucagon in a lipid–water interphase by ^{1}H nuclear magnetic resonance. *J Mol Biol* **169**: 921–948, 1983.
2. Havel TF and Wüthrich K, An evaluation of the combined use of nuclear magnetic resonance and distance geometry for the determination of protein conformations in solution. *J Mol Biol* **182**: 281–294, 1985.
3. Clore GM, Gronenborn AM, Brunger AT and Karplus M, Solution conformation of a heptadecapeptide comprising the DNA binding helix F of the cyclic AMP receptor protein of *Escherichia coli:* Combined use of ^{1}H nuclear magnetic resonance and restrained molecular dynamics. *J Mol Biol* **186**: 435–455, 1985.

4. Holak TA, Keasely SK, Kim Y and Prestegard JH, The three dimensional structure of acyl carrier protein determined by NMR-pseudoenergy and distance geometry calculations. *Biochemistry* **27**: 6135–6142, 1988.
5. Kline AD, Braun W and Wüthrich K, Determination of the complete three-dimensional structure of the α-amylase inhibitor tendamistat in aqueous solution by nuclear magnetic resonance and distance geometry. *J Mol Biol* **204**: 675–724, 1988.
6. Moore JM, Case DA, Chazin WJ, Gippert GP, Havel TF, Powls R and Wright PE, Three-dimensional solution structure of plastocyanin from the green alga *Scenedesmus obliquus*. *Science* **240**: 314–317, 1988.
7. Clore GM, Gronenborn AM, Nilges M and Ryan CA, Three-dimensional structure of potato carboxypeptidase inhibitor in solution: A study using nuclear magnetic resonance, distance geometry, and restrained molecular dynamics. *Biochemistry* **26**: 8012–8023, 1987.
8. Wagner G, Braun W, Havel TF, Schaumann T, Go W and Wüthrich K, Protein structures in solution by nuclear magnetic resonance and distance geometry: The polypeptide fold of the basic pancreatic trypsin inhibitor determination using two different algorithms, DISGEO and DISMAN. *J Mol Biol* **196**: 611–639, 1987.
9. Ohlrogge JB, Biochemistry of plant acyl carrier proteins. In: *The Biochemistry of Plants* (Ed. Stumpf PK), Vol. 9, pp. 137–157. Academic Press, Orlando, FL, 1987.
10. Kuo TM and Ohlrogge JB, The primary structure of spinach acyl carrier protein. *Arch Biochem Biophys* **234**: 290–296, 1984.
11. Simoni RD, Criddle RS and Stumpf PK, Fat metabolism in higher plants. *J Biol Chem* **242**: 573–581, 1967.
12. Ohlrogge JB, Shine WE and Stumpf PK, Fat metabolism in higher plants. Characterization of plant acyl-ACP and acyl-CoA hydrolases. *Arch Biochem Biophys* **189**: 382–391, 1978.
13. Kim Y and Prestegard JH, A dynamic model for the structure of acyl carrier protein in solution. *Biochemistry* **28**: 8792–8797, 1989.
14. Guerra DJ, Dziewanowska K, Ohlrogge JB and Beremand PD, Purification and characterization of recombinant spinach acyl carrier protein I expressed in *Escherichia coli*. *J Biol Chem* **263**: 4386–4391, 1988.
15. LeMaster DM, Kay LE, Brünger AT and Prestegard JH, Protein dynamics and distance determination by NOE measurements. *FEBS Lett* **236**: 71–76, 1988.
16. Folkers PJM, Clore GM, Driscoll PC, Dodt J, Köhler S and Gronenborn AM, Solution structure of recombinant hirudin and the Lys-47 → Glu mutant: A nuclear magnetic resonance and hybrid distance geometry–dynamical simulated annealing study. *Biochemistry* **28**: 2601–2617, 1989.
17. Scarsdale JN, Ram P, Yu RK and Prestegard JH, A molecular mechanics–NMR pseudoenergy approach to the solution conformation of glycolipids. *J Computat Chem* **9**: 133–147, 1988.
18. Rock CO and Garwin JL, Preparative enzymatic synthesis and hydrophobic chromatography of acyl-acyl carrier protein. *J Biol Chem* **254**: 7123–7128, 1979.
19. Wider G, Macura S, Kumar A, Ernst RR and Wüthrich K, Homonuclear two-dimensional ^{1}H NMR of proteins. Experimental procedures. *J Magn Reson* **56**: 207–234, 1984.
20. States DJ, Haberkorn Γ \ and Ruben DJ, A two-dimensional nuclear Overhauser experiment with pure absorption phase in four quadrants. *J Magn Reson* **48**: 286–292, 1982.
21. Bodenhausen G, Vold RL and Vold RR, Multiple quantum spin-echo spectroscopy. *J Magn Reson* **37**: 93–106, 1980.
22. Redfied AG and Kunz SD, Quadrature fourier NMR detection: Simple multiplex for dual detection and discussion. *J Magn Reson* **19**: 250–254, 1975.
23. Bax A and Drobny G, Optimization of two-dimensional homonuclear relayed coherence transfer NMR spectroscopy. *J Magn Reson* **61**: 306–320, 1985.
24. Yang JT, Wu CC and Martinez HM, Calculation of protein conformation from circular dichroism. *Methods Enzymol* **130**: 208–265, 1986.
25. Holak TA, Nilges M, Prestegard JH, Gronenborn AM and Clore GM, Three-dimensional structure of acyl carrier protein in solution determined by nuclear magnetic resonance and the combined use of dynamical simulated annealing and distance geometry. *Eur J Biochem* **175**: 9–15, 1988.
26. Holak TA, Nilges M and Oschkinat H, Improved strategies for the determination of protein structures from NMR data: The solution structure of acyl carrier protein. *FEBS Lett* **242**: 218–224, 1989.
27. Kuo TM and Ohlrogge JB, A novel, general radioimmunoassay for acyl carrier proteins. *Anal Biochem* **136**: 497–502, 1984.
28. Chou PY and Fasman GD, Conformational parameters for amino acids in helical, β-sheet, and random coil regions calculated from proteins. *Biochemistry* **13**: 211–221, 1974.
29. Chou PY and Fasman GD, Prediction of protein conformation. *Biochemistry* **13**: 222–245, 1974.
30. Chou PY and Fasman GD, Empirical predictions of protein conformation. *Annu Rev Biochem* **47**: 251–276, 1978.
31. Rock CO and Cronan JE Jr, Re-evaluation of the solution structure of acyl carrier protein. *J Biol Chem* **254**: 9778–9785, 1979.
32. Schulz H, On the structure–function relationship of acyl carrier protein of *Escherichia coli*. *J Biol Chem* **250**: 2299–2304, 1975.
33. Schulz H, Increased conformational stability of *Escherichia coli* acyl carrier protein in the presence of divalent cations. *FEBS Lett* **78**: 303–306, 1977.
34. Wüthrich K, *NMR of Proteins and Nucleic Acids*. John Wiley, New York, 1986.
35. Bothner-By AA, Stephens RL, Lee JM, Warren CD and Jeanloz RW, Structure determination of a tetrasaccharide: Transient nuclear Overhauser effects in the rotating frame. *J Am Chem Soc* **106**: 811–813, 1984.
36. Bax A and Davis DG, Practical aspects of two-dimensional transverse NOE spectroscopy. *J Magn Reson* **63**: 207–213, 1985.
37. Bax A, Correction of cross-peak intensities in 2D spin-locked NOE spectroscopy for offset and Hartmann–Hahn effects. *J Magn Reson* **77**: 134–147, 1988.